Ab initio molecular dynamics with an orbital-free density functional

1993 J. Phys.: Condens. Matter 5 3221

(http://iopscience.iop.org/0953-8984/5/19/019)

J. Phys.: Condens. Matter 5 (1993) 3221–3240. Printed in the UK

Ab initio molecular dynamics with an orbital-free density functional

M Pearson, E Smargiassi and P A Madden
Physical Chemistry Laboratory, Oxford University, South Parks Road, Oxford OX1 3QZ, UK

Received 29 January 1993, in final form 16 March 1993

Abstract. A scheme for *ab initio* simulations of extended systems, which involves the use of the electron density as the basic variable, is discussed. The form of the kinetic energy functional is chosen to incorporate several exact limits (uniform system, linear response and rapidly varying density) while the rest of the energy functional is exactly the same as in a Kohn–Sham density functional calculation with the local density approximation. We show that for sodium the present scheme yields high-quality results in a fraction of the time required with an orbital-based functional. The electronic part of the algorithm scales linearly with system size. An analysis of the stability of the method is made, and leads to criteria for selecting the non-physical parameters in the calculation so as to maximize the computational efficiency.

1. Introduction

The *ab initio* molecular dynamics technique [1], introduced by Car and Parrinello (CP), enables the simulation of multinuclear systems on an adiabatic electronic energy surface calculated 'on the fly'. The method thereby avoids the introduction of an effective potential energy, expressed as a function of the internuclear coordinates, and thus greatly broadens the range of physical systems accessible to simulation methods. The CP formalism is also at the heart of efficient methods for performing total energy minimizations on condensed matter systems [2].

Most successful applications of the method have made use of a density functional prescription for calculating the electronic energy. The use of the electron density $\rho(\boldsymbol{r})$ as the basic variable in the description of the electronic state is sanctioned by the Hohenberg–Kohn theorem [3]. In practical calculations [4–6] the Kohn–Sham (KS) [7] realization of the formalism is used in which the energy functional, $E[\rho(\boldsymbol{r})]$ is expressed as the sum of kinetic, Coulomb (Hartree), exchange-correlation and external functionals:

$$E[\rho] = E_{\mathrm{KE}}[\rho] + E_{\mathrm{Hart}}[\rho] + E_{\mathrm{xc}}[\rho] + E_{\mathrm{ext}}[\rho]. \tag{1.1}$$

The kinetic energy functional is the kinetic energy of a *non-interacting* electron gas with the same density as that of the interacting system of interest. In order to represent this kinetic energy functional for N electrons, a set of N orthonormal orbitals are introduced such that

$$\rho(\boldsymbol{r}) = \sum_{i=1}^{N} \psi_i(\boldsymbol{r})^* \psi_i(\boldsymbol{r}) \tag{1.2}$$

and

$$E_{\mathrm{KE}} = \sum_i \int \mathrm{d}\boldsymbol{r}\ \psi_i(\boldsymbol{r})^* (-\tfrac{1}{2}\nabla^2) \psi_i(\boldsymbol{r}). \tag{1.3}$$

0953-8984/93/193221+20$07.50

With this form chosen for E_{KE}, very useful expressions for E_{xc} have been determined [4] which are the basis for a successful description of the electronic ground state of condensed [8,9] and molecular [10,11] systems. Furthermore, there has been much work done to obtain accurate and transferable pseudopotentials [12,13] (V_{el}) to describe the interaction of the ion cores with the valence electrons in the KS scheme; these appear in $E_{ext}[\rho]$:

$$E_{ext} = \int d\boldsymbol{r}\rho(\boldsymbol{r})V_{ext}(\boldsymbol{r}) \tag{1.4}$$

with

$$V_{ext}(\boldsymbol{r}) = \int d\boldsymbol{r}'\ V_{el}(\boldsymbol{r}-\boldsymbol{r}')\sum_{\alpha=1}^{N_I}\delta(\boldsymbol{r}'-\boldsymbol{R}_\alpha) \tag{1.5}$$

where the sum runs over ions.

In the CP formalism, use of the KS representation leads to a set of N functional differential equations that describe the time evolution of the electronic state [14,15] as the ions move. In practice, the orbitals are expanded in a set of M basis functions, usually plane waves, so that a set of $N \times M$ time differential equations result. The right-hand sides of these equations contain the effect of the Hamiltonian on the orbitals and a set of constraint forces, which serve to keep the occupied orbitals orthonormal. With plane waves as basis functions, evaluation of the Hamiltonian can be made very efficient. In favourable circumstances, the computational cost of evaluating this term scales as $NM\ln M$. Since M may be a large number $\simeq 10^4$ this factor normally determines the expense of the calculation. For a given physical system both N and M increase linearly with the volume (Ω) of the system, if the same plane-wave cutoff g_c is maintained. Consequently, the evaluation of the Hamiltonian scales as $\Omega^2\ln\Omega$. However, for very large calculations, the most time-consuming part becomes the imposition of the orthonormality constraints, which scale with Ω^3. In a straightforward implementation of the CP scheme, it is then the scaling properties of the orbital orthogonalization that limits the size of system which may be tackled. Very recently, there have been attempts to devise modified algorithms with better scaling properties, within the Kohn–Sham representation [16,17].

When viewed from a distance the finding that this orthogonality problem limits the applicability of the CP method seems bizarre. The orbitals were only introduced to represent the kinetic energy of *non-interacting* electrons; this would seem to be a trivial part of the totality of the electronic energy compared to the complexities that are contained within E_{xc}! The most attractive way out of the dilemma appears to be to invoke the full power of the Hohenberg–Kohn theorem and find a sufficiently good representation of the non-interacting kinetic energy E_{KE}, which is a functional only of $\rho(\boldsymbol{r})$ itself. We would then combine this with the Coulomb, exchange-correlation and external energy functionals that have been developed within the Kohn–Sham realization and whose success is now well established.

Given such a functional we could construct a variant of the original CP scheme. Consider, for example, a system of N electrons and N_I ions in a cubic cell of length L. The electron density is periodic and may be expanded as a Fourier series

$$\rho(\boldsymbol{r}) = \sum_{\boldsymbol{g}}\rho_{\boldsymbol{g}}e^{i\boldsymbol{g}\cdot\boldsymbol{r}} \tag{1.6}$$

where $\boldsymbol{g} = (2\pi/L)[l,m,n]$, l,m,n are integers such that $g \leqslant g_c$. By following the normal routes (as in [15], for example) to the derivation of the CP equations, with these Fourier

coefficients of the electron density, ρ_g, as the additional dynamical variables that prescribe the electronic state, we readily obtain the coupled equations for the ion position ($\boldsymbol{R}_\alpha$) and coefficient dynamics:

$$\mu_g \ddot{\rho}_g = -\frac{\delta E}{\delta \rho_g} \qquad g \leqslant g_c \tag{1.7}$$

where μ_g is a 'fake mass' or inertia parameter, and

$$M_I \ddot{\boldsymbol{R}}_\alpha = -\nabla_\alpha E - \nabla_\alpha V_{II} \qquad \alpha = 1, N_I \tag{1.8}$$

where V_{II} is the potential energy of the direct ion–ion interaction. These equations differ from the normal CP equations in two ways. There are M equations of type (1.7) rather than the $N \times M$ orbital coefficient equations found with the KS functional: we would therefore expect the cost of evaluating the Hamiltonian to be a factor N smaller than in this case. Secondly, (1.7) contains no constraint terms; the only constraint to be implemented is simply that the total number of electrons is conserved:

$$\rho_{g=0} = N/\Omega \tag{1.9}$$

(which is imposed on all the Fourier space equations below). From these considerations, we anticipate an algorithm that scales as $\Omega \ln \Omega$, i.e. roughly linearly with system size. In addition the memory requirements will scale linearly with Ω rather than quadratically, as in the orbital-based calculation.

The objective of this paper is to show that these possibilities are largely realised, at least for simple metals, and that there are further practical advantages, not anticipated in the discussion above, which make such a scheme even more attractive than outlined for metallic systems.

Firstly, we show that a kinetic energy functional can be constructed which gives results for the properties of simple metals that are as good as those obtained from the KS formalism. The energy functional is constructed by following the suggestions of Perrot [18], but a closely related functional has recently been introduced by Wang and Teter [19], who also demonstrate the possibilities for further systematic improvements, which will extend the range of physical systems that can be represented with an orbital-free density functional. A point to note here is that, to obtain accurate KS results for metals, it is often necessary to employ Brillouin-zone sampling (see [15] for a discussion); this is necessary to get a good representation of the *wavefunction*—the density is unaffected. In effect, then, smaller basis sets are required in orbital-free DFT calculations—a factor that becomes particularly important in disordered systems or dynamics runs, when symmetry cannot be invoked to reduce the number of sampling points.

Secondly, we show that the coupled equations above do update the adiabatic ground electronic state in the desired manner as the ions move. In fact, as we will demonstrate, for metals the adiabatic update takes place far more readily (i.e. *without* re-quenching or thermostatting [20, 21]) in the true DFT scheme than within the KS description. Furthermore, it becomes possible to 'condition' the coefficient equations (1.7), by a predetermined choice of the μ_g, so that an optimum timestep for dynamics may be chosen *approaching the natural MD timestep for the ionic system.* Consequently, the real time evolution is extremely rapid.

Although the scaling argument, which was outlined above, *is* borne out by the results we find, in practice, that it is incomplete. The electron–ion interaction, which is a minor contributor to the computational cost of a KS-based calculation (and therefore neglected in the argument presented), becomes the slowest part of the true DFT calculation for large system sizes. Although this, at present, seems to prevent us (or anyone) reaching the Holy Grail of a linear scaling algorithm, it does emphasize how rapidly the rest of the calculation can be made to proceed.

2. The choice of kinetic energy functional

There have been previous formulations [22, 23] of CP algorithms based upon the Thomas–Fermi kinetic energy functional [4–6]

$$E_{\mathrm{TF}}[\rho] = \tfrac{3}{10}(3\pi^2)^{2/3}\int_{\Omega} \mathrm{d}r\ \rho(r)^{5/3}. \tag{2.1}$$

By construction, this gives the exact energy of a uniform non-interacting electron gas. It is also known to become exact for atoms in the limit of infinite nuclear charge and also in the limit of high electron density. Because of the latter property, the Thomas–Fermi functional becomes useful in the description of some plasmas [22]. However, from a consideration of the effective response properties of the electronic system described by this functional, it can readily be seen that we must improve on $E_{\mathrm{TF}}[\rho]$ to get an adequate description of the effective ion–ion interactions in metals.

2.1. Linear response and the kinetic energy functional

In the conventional picture, the direct ion–ion interactions are screened by the perturbations in the electron gas induced by the electron–ion interactions. If these interactions are weak, the induced charge density is calculated from the linear response of the electron gas to the electron–ion potential (V_{ext}) [24]. In Fourier space

$$\rho_g = F(g)V_{\mathrm{ext}}(g) \tag{2.2}$$

where $F(g)$ is the *external* response function (or susceptibility). Alternatively, the electron gas may be regarded as responding to the total potential, consisting of V_{ext} plus the potential due to the charge density induced by the external field. In this case

$$\rho_g = \chi(g)\big(V_{\mathrm{ext}}(g) + V_{\mathrm{ind}}(g)\big) \tag{2.3}$$

where $\chi(g)$ is called the screened response function (or screened susceptibility). The susceptibilities associated with a given choice of kinetic energy functional are readily obtained. The equilibrium-induced density for a given external disturbance is obtained by minimizing the energy functional with respect to variations in the charge density; for the TF functional

$$\frac{\delta E}{\delta\rho(r)} = \tfrac{1}{2}\big(3\pi^2\rho(r)\big)^{2/3} + V_{\mathrm{ext}}(r) + V_{\mathrm{ind}}(r) = 0 \tag{2.4}$$

where

$$V_{\mathrm{ind}}(r) = \frac{\delta E_{\mathrm{Hart}}}{\delta\rho(r)} + \frac{\delta E_{\mathrm{xc}}}{\delta\rho(r)}. \tag{2.5}$$

For small perturbations about a uniform density we may linearize the kinetic energy gradient, giving

$$\frac{\delta E}{\delta\rho(r)} = \frac{\pi^2}{k_{\mathrm{F}}}\delta\rho(r) + V_{\mathrm{ext}}(r) + V_{\mathrm{ind}}(r) = 0 \tag{2.6}$$

where k_F is the Fermi wavevector for the uniform system ($k_F = (3\pi^2\rho_0)^{1/3}$). In reciprocal space, this is

$$\frac{\delta E}{\delta \rho_g} = \frac{\pi^2}{k_F}\rho_g + V_{ext}(g) + V_{ind}(g) = 0 \qquad g \neq 0. \tag{2.7}$$

Comparing with (2.3) we see that the screened susceptibility implicit in the choice of Thomas–Fermi functional is a constant:

$$\chi_{TF}(g) = -\frac{k_F}{\pi^2}. \tag{2.8}$$

In the simplest case, where the exchange-correlation contributions are neglected (i.e. a 'Hartree' gas), this response function leads to the prediction that the screened potential due to a point-charge ion is of Yukawa form [25, 26].

However, for this system the exact screened-response function is the Lindhard function [27]:

$$\chi_0(g) = -\frac{k_F}{\pi^2}\left(\frac{1}{2} + \frac{1-q^2}{4q}\ln\left|\frac{1+q}{1-q}\right|\right) \tag{2.9}$$

where $q = g/2k_F$. The Lindhard and Thomas–Fermi response functions, χ_0 and χ_{TF}, are equal in the limit of low q. For larger q, however, χ_0 is considerably less negative than χ_{TF}, i.e. Thomas–Fermi theory overestimates the response. At $q = 1$ ($g = 2k_F$) the Lindhard function has a logarithmic singularity in the derivative (which is due to the discontinuity in the occupation of the electron levels at the Fermi surface). The result of this is that the screened potential of a point charge has considerably more structure than the simple Yukawa potential predicted by TF theory. In particular, it can be shown (e.g. [25, 26]) that at large distances, the screened potential does not simply decay exponentially, as with the Yukawa potential, but instead has a slowly decaying oscillatory term:

$$V_{scr}(r) \sim \frac{1}{r^3}\cos 2k_F r. \tag{2.10}$$

These so-called *Friedel oscillations* in $V_{scr}(r)$ are an important aspect of the effective interionic interactions in metals [26, 28].

Hohenberg and Kohn (HK) [3, 29] showed how to construct a kinetic energy functional for non-interacting fermions that yields the correct linear response behaviour. For a uniform non-interacting electron gas the kinetic energy is given by the Thomas–Fermi result (2.1); for small departures from uniformity, the energy may be expanded in the Fourier coefficients of the density fluctuations†

$$E_{KE} = E_{TF}(\rho_0) + \frac{\Omega}{2}\sum_{g\neq 0}\rho_g\rho_g^* K(g) \tag{2.11}$$

where the absence of a linear term follows from the equilibrium condition. For non-interacting electrons the total energy is

$$\begin{aligned} E[\rho] &= E_{KE}[\rho] + E_{ext}[\rho] \\ &= E_{TF}(\rho_0) + \frac{\Omega}{2}\sum_{g\neq 0}\rho_g\rho_g^* K(g) + \Omega\sum_g V_{ext}(g)^*\rho_g \end{aligned} \tag{2.12}$$

† The apparently mysterious appearance of the Ω factor here is related to the fact that we *sum* over points g in reciprocal space and integrate over real space r.

and so at equilibrium

$$\frac{\delta E}{\delta \rho_g} = \rho_g \; K(g) + V_{\text{ext}}(g) = 0. \tag{2.13}$$

Hence, by choosing K to be minus the reciprocal of the exact *external* susceptibility of the non-interacting electron gas, the correct response properties are guaranteed for this case. However, the susceptibility for this case is also the Lindhard function $\chi_0(g)$ [27] and so

$$E_{\text{HK}} = E_{\text{TF}}(\rho_0) + \frac{1}{2}\sum_{g\neq 0} \rho_g \rho_g^* \left(-\frac{\Omega}{\chi_0(g)}\right). \tag{2.14}$$

If we now examine the consequences of this choice for the Hartree gas we find

$$\frac{\delta E}{\delta \rho_g} = \rho_g \left(-\frac{1}{\chi_0(g)}\right) + V_{\text{ext}}(g) + V_{\text{ind}}(g) = 0 \tag{2.15}$$

i.e. that the predicted *screened* response function for this case is the Lindhard function—which is the correct result [27]. Using the Hohenberg–Kohn functional for the kinetic energy functional of the non-interacting electron gas will therefore give the Friedel oscillations in the effective interactions between ions.

2.2. *Results with the Hohenberg–Kohn functional*

As stated in the introduction, the objective is to combine the kinetic energy functional with forms for exchange-correlation and external functionals, which have been determined within the Kohn–Sham formulation. With the HK kinetic energy functional, (1.7) becomes

$$\mu_g \ddot{\rho}_g = -\frac{\delta E}{\delta \rho_g} = \left(-\frac{1}{\chi_0(g)}\right)\rho_g + (4\pi/g^2)\rho_g + V_{\text{ext}}(g) + \frac{\delta E_{\text{xc}}}{\delta \rho}(g). \tag{2.16}$$

The second term on the right-hand side is the Coulomb (Hartree) potential; the third is the external potential

$$V_{\text{ext}}(g) = \sum_{\alpha} V_{\text{el}}(g) e^{ig\cdot R_\alpha} \tag{2.17}$$

where the sum runs over ions and V_{el} is the pseudopotential. The final term is the exchange-correlation potential, we used the Ceperley–Alder [30] function (as parametrized in [31]) for E_{xc}. The term $\delta E_{\text{xc}}/\delta\rho(r)$ is evaluated from the density in real space and then Fourier transformed. Equation (2.16) is therefore readily evaluated at the cost of two fast Fourier transformations.

The first thing we sought to establish was whether the linear response characteristics of this total functional agreed with the known response characteristics of the interacting electron gas *including* exchange and correlation. In the construction of effective interion potentials an external response function of the form

$$F(g) = \chi_0(g)/[1 + (4\pi/g^2)(G(g) - 1)\chi_0(g)] \tag{2.18}$$

is used, where $G(g)$ is a 'local field factor', which accounts for the exchange and correlation effects. ($G(g) = 0$ gives the correct relationship between external and screened response

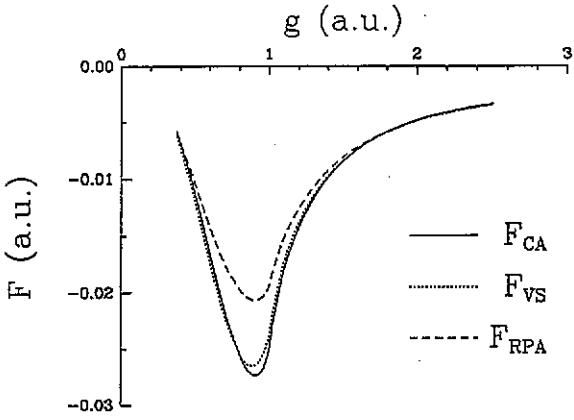

Figure 1. A comparison of external susceptibilities obtained from the random phase approximation (i.e. for the Hartree gas—denoted RPA), including exchange and correlation effects using the Vashista–Singwi local-field factor (VS) and the effective external susceptibility implicit in the present calculations using the Ceperley–Alder exchange-correlation functional (CA). Note that $k_F = 0.49$ au for solid Na.

function for the Hartree gas [27]). An accurate local field factor is believed to be that of Vashista and Singwi [32], and this is widely used [28]. We can compute the external response function for the chosen functional by solving (2.16) with $\ddot{\rho}_g = 0$ in the presence of an arbitrary weak form for $V_{ext}(g)$, and comparing $\rho_g / V_{ext}(g)$ with values of $F(g)$ from (2.18). The result is shown in figure 1; the two curves are in excellent agreement and appreciably different to the external response function for the Hartree gas. We may therefore be confident that the linear response properties of the electronic system represented by our chosen density functional are as good as those used as an input to effective potential calculations.

Next, we attempted to use the HK kinetic energy functional in calculations on sodium. For the external energy functional we use the norm-conserving local pseudopotential of Topp and Hopfield [33], which was determined within the Kohn–Sham representation and is known to give a good account of the properties of sodium [34]. The ions were placed in their crystalline lattice positions and we attempted to minimize the energy functional by varying the ρ_g from a random initial starting point. These calculations rapidly became unstable—this could be traced to the fact that the electron density was becoming negative at points in real space at which the external potential was appreciably negative (i.e. repulsive for electrons). In the KS scheme the density is constrained to be positive, since it is expressed as the square modulus of the wavefunction; in our calculations this is not so and the system tends towards an unphysical minimum with negative electron densities. Similar behaviour has been noted using the TF functional with strong external potentials [23].

Our prescription for the external energy is driven by the objective described in section 1: to take all aspects of the density functional, except E_{KE}, from work based upon the Kohn–Sham representation and thereby confer '*ab initio*' respectability and transferability on our calculations. The negative density problem must therefore be viewed as a shortcoming of E_{KE}. With a functional that is quadratic in the density fluctuations, the force that resists the passage into the negative density region does not increase sufficiently rapidly as the density becomes very small.

These findings appear to throw up a paradox: the motivation we presented for incorporating correct linear response in our functional was the fact that successful effective interionic potentials for metals (including sodium) are constructed by calculating the screening by the induced charge density on the basis of the linear response of the electron gas to the electron–ion interaction. We now find that the *actual* response of the valence electrons is much too strong to be described by linear response theory! The resolution of this 'paradox' lies in the character of the pseudopotentials used. We used an *ab initio*

potential, which can be taken to represent the true strength of the interaction between the ion cores and the valence electrons, whereas in the construction of effective interion potentials empirical pseudopotentials are used and parameters in them are determined by requiring that the properties of the bulk ionic system agree with experiment. In this procedure it is *assumed* that linear response is adequate, and the consequences of this assumption are bound into the values of the fitted parameters. In practice, this means that the effective interion potentials are not transferable.

2.3. The 'Perrot' functional

An important improvement in the properties of the functional described above can be obtained by combining it with the von Weizsäcker functional [35]:

$$E_{\mathrm{vW}}[\rho] = E_{\mathrm{TF}}[\rho] + \frac{1}{8}\int_{\Omega} \frac{\nabla\rho(r)\cdot\nabla\rho(r)}{\rho(r)}. \tag{2.19}$$

(In fact, in von Weizsäcker's original argument, $E_{\mathrm{TF}}[\rho]$ does not appear, and consequently his functional does not give the correct energy for a uniform system; we will refer to (2.19) as the von Weizsäcker functional for convenience.) The functional derivative of E_{vW} is

$$\frac{\delta E_{\mathrm{vW}}}{\delta\rho(r)} = \tfrac{1}{2}(3\pi^2)^{2/3}\rho(r)^{2/3} + \frac{1}{8}\frac{\nabla\rho(r)\cdot\nabla\rho(r)}{\rho(r)^2} - \frac{1}{4}\frac{\nabla^2\rho(r)}{\rho(r)}. \tag{2.20}$$

By adopting $E_{\mathrm{vW}}[\rho]$ as the kinetic energy functional in (2.4) we can follow the procedure outlined above for the Thomas–Fermi functional and extract the effective linear response function for the Hartree gas. This was first presented by Jones and Young [36]:

$$\chi_{\mathrm{vW}}(g) = -\frac{k_{\mathrm{F}}}{\pi^2}\left(\frac{1}{1+3q^2}\right) \tag{2.21}$$

where $q = g/2k_{\mathrm{F}}$. It behaves asymptotically as

$$\chi_{\mathrm{vW}}(g) = \begin{cases} -(k_{\mathrm{F}}/\pi^2)(1-3q^2) & q \to 0 \\ -(k_{\mathrm{F}}/\pi^2)(1/3q^2) & q \to \infty. \end{cases} \tag{2.22}$$

The true linear response, however, is given by the Lindhard function (2.9), which behaves asymptotically as

$$\chi_0(g) = \begin{cases} -(k_{\mathrm{F}}/\pi^2)(1-q^2/3) & q \to 0 \\ -(k_{\mathrm{F}}/\pi^2)(1/3q^2) & q \to \infty. \end{cases} \tag{2.23}$$

A comparison of χ_{vW} and χ_0 shows that χ_{vW} gives the correct linear response in the limit of large q. (The correct low-q behaviour would be obtained if the integral in (2.19) were multiplied by a factor of 1/9; this gives the normal gradient correction to TF [4].) In fact, it is believed that, in the limit of large q, the von Weizsäcker functional is exact not only in the linear response régime, but for all perturbations [6]. (Although no general proof has been provided for this, it has been proven to be the case for a number of special situations e.g. under the locally linear potential approximation, for a single particle, in the $r \to 0$ and $r \to \infty$ limits for atoms [6].)

Perrot [18] has suggested that a kinetic energy functional that combines the attractive properties of the von Weizsäcker and Hohenberg–Kohn functionals can be constructed by building the correct linear response into the von Weizsäcker form, i.e.

$$E_{\mathrm{P}}[\rho] = E_{\mathrm{vW}}[\rho] - E_{\mathrm{lin}}[\rho] + E_{\mathrm{HK}}[\rho] \tag{2.24}$$

where E_{lin} is the linearized form of E_{vW} and E_{HK} is the Hohenberg–Kohn linear response functional; i.e.

$$E_{\mathrm{P}}[\rho] = E_{\mathrm{TF}}[\rho] + \frac{1}{8}\int_{\Omega}\frac{\nabla\rho(\boldsymbol{r}).\nabla\rho(\boldsymbol{r})}{\rho(\boldsymbol{r})} + \frac{\Omega}{2}\sum_{g}\rho_g\rho_g^*\left(\frac{1}{\chi_{\mathrm{vW}}(g)} - \frac{1}{\chi_0(g)}\right). \tag{2.25}$$

The Perrot functional thus has the properties that it gives the correct linear response for all q (since for small perturbations $E_{\mathrm{vW}} = E_{\mathrm{lin}}$) and that it is believed to be asymptotically exact in the limit of large q (since as $q \to \infty$, $E_{\mathrm{lin}} \to E_{\mathrm{HK}}$) for perturbations of all sizes. It is this latter attribute that should serve to prevent the 'negative density' problem encountered with E_{HK} alone. The von Weizsäcker functional can be derived on an essentially one-electron picture—by considering the 'Schrödinger equation' for the square root of the density. As such it contains no account of Fermi statistics; E_{HK}, on the other hand, has the correct statistics built in (for the uniform system and at the level important for linear response)—as we emphasized, these have important consequences for metallic behaviour. We can hope that the combination contains sufficient ingredients to give realistic interionic interactions in metals.

We note that a different functional with these same properties has recently been proposed by Wang and Teter [19]. Wang and Teter also described ways of constructing a functional that is correct to *third* order in the density fluctuations. We have conducted a numerical study, of the type described below, of the properties of the Perrot and Wang-Teter second-order functionals and found very little to choose between them. As we will see below, these second-order functionals are already sufficiently close to reality to permit the properties of simple metals to be modelled accurately.

3. Results for solid sodium

In this section we describe results obtained for solid sodium using the Perrot kinetic energy functional, the Topp–Hopfield pseudopotential and the Ceperley–Alder exchange-correlation term. In all calculations a plane-wave cutoff of 9.8 Ryd was used.

3.1. The BCC lattice parameter and bulk modulus

Calculations were performed on a 54-atom cell (i.e. a $3 \times 3 \times 3$ array of two-atom body-centred cubic unit cells). Starting from a random electronic configuration, an energy minimization was performed for the sodium BCC lattice at the experimental lattice parameter $a = 7.984$ au. Having obtained the ground state for the experimental geometry, the energy of the sodium lattice was then minimized with respect to the BCC cell parameter a. The results are shown in figure 2. The minimum energy is achieved with $a = 8.141$ au (2.0% higher than the experimental value of 7.984 au).

The Perrot result was compared with that from a KS calculation on the same 54-atom cell, again with a 9.8 Ryd energy cutoff. Only the Γ point was included in the sampling scheme. This calculation gives a lattice parameter of 8.06 au (1.0% higher than the experimental

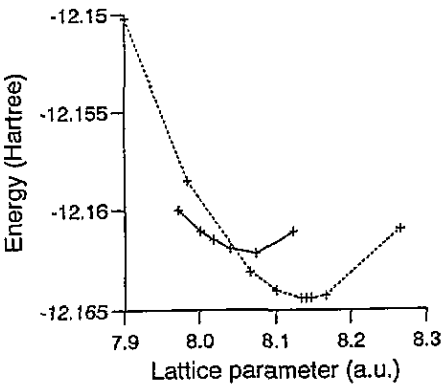

Figure 2. The variation of the total energy with lattice parameter for sodium in the present calculations (broken curve) and from a Γ point Kohn–Sham calculation on a 54-atom cell [34] (full curve).

value). The absolute values for the total energy differ considerably between the Perrot and KS calculations. This discrepancy can be traced to the fact that a finite-size Γ-point Kohn–Sham calculation does not give the correct energy for a uniform electron gas (whereas the Perrot functional is correct by construction). When the Kohn–Sham energy is adjusted by subtracting the difference between the free-electron gas energy obtained from a 54-electron Γ-point Kohn–Sham calculation and the exact value (0.145 hartrees), the agreement between the Perrot and Kohn–Sham energies is correct to within 0.003 hartrees. It is the shifted Kohn–Sham curve that is shown in figure 2.

From this data we may also extract a value for the bulk modulus of sodium. We obtain 6.5×10^{10} dyne cm^{-2}, using the Perrot functional, against an experimental value [26] of 6.4×10^{10} dyne cm^{-2}, an error of less than 2%.

3.2. Vacancy formation energy

A calculation of the energy to form a vacancy is a non-trivial test of the reliability of the model of effective interactions in a material. Pair potentials necessarily lead to the prediction that the vacancy formation energy is equal to the heat of sublimation per atom; these two quantities normally correlate poorly [26].

We have obtained the vacancy formation energy from the total energies of 54- and 53-atom systems (E_c and E_v, respectively) with a simulation cell length of 23.952 au, which gives the experimental density at $T = 0$. The ions were allowed to relax in the 53-atom calculation, the relaxation energy was 0.1 eV. The formation energy E_f is obtained from

$$E_f(T = 0) = E_v - (53/54)E_c = 0.3\,\text{eV} \tag{3.1}$$

which should be compared with an experimental value of $\simeq 0.4$ eV [37, 38]. A KS calculation on the same system using only the Γ point in the sampling scheme and without allowing for ionic relaxation has also been performed [34]. This gives a value of 0.7 eV, substantially worse than the value obtained using the Perrot functional, presumably because of poor sampling.

We have also estimated the activation energy for vacancy migration by calculating the energy of the split vacancy (including ionic relaxation), as above, and subtracting from it the vacancy formation energy. This gives a value of 0.03 eV compared with an experimental upper bound of 0.1 eV obtained from self-diffusion data [39, 40].

3.3. Sodium lattice dynamics

We carried out a set of molecular dynamics runs on the sodium lattice at a temperature of 25 K in order to establish the phonon dispersion curves predicted by the Perrot functional. The lattice parameter was set at the experimental value of 7.984 au. The initial ionic velocities were drawn randomly from a Maxwell–Boltzmann distribution at $T = 50$ K. A leapfrog Verlet algorithm [41] was used for both the ionic and coefficient equations. The coefficient velocities were initialized by performing a backstep from the initial configuration [15].

Short test runs were carried out to establish optimum values for the timestep and 'fake mass' parameters μ_g. In the work described in this section, μ_g took the g-independent value μ. As we will discuss in more detail below, the criterion for choosing these values is that the dynamics should be 'adiabatic', i.e. that the system should remain in the electronic ground state during the dynamics run. This is achieved by choosing a small value for μ. On the other hand, a very small value for μ necessitates a small value for δt, in order that the rapid oscillations associated with the electronic system (whose frequency scales as $\mu^{-1/2}$) are followed by the integration procedure. We settled on values of $\delta t = 40$ atu ($= 9.7 \times 10^{-16}$ s) and $\mu = 1.4 \times 10^6$ au (note that the term 'fake mass' is somewhat misleading; with the electronic equations written as in (1.7), μ has dimensions of energy $\times$ volume $\times$ time^2).

Having optimized μ and δt, relatively long CP runs were carried out in order to obtain the phonon dispersion curves for sodium. The runs were 2000 steps in length, giving a total simulation time of 80 000 atu (about 2 ps).

The variation of the components of the total energy during a 54-atom run are shown in figure 3. The CP algorithm is seen to be stable right up to the end of the run. The start-up is good (there are no high-frequency oscillations in the fake kinetic energy) and the total energy is conserved to a high degree of accuracy. At the start of the run, the ion temperature drops from 50 K to about 25 K, as the energy in the ionic vibrations (initially all kinetic) becomes partitioned equally between kinetic and potential. There is no apparent energy exchange between the electronic and ionic degrees of freedom during the run. The drift off the Born–Oppenheimer surface is 0.59×10^{-7} hartrees (for the 128-atom calculation it is 0.838×10^{-6} hartrees).

In order to calculate the phonon dispersion curves we calculate the longitudinal and transverse current correlation functions

$$C^{\mathrm{l}}(q,t) = \left\langle \left(\sum_{I=1}^{N} \frac{\boldsymbol{q} \cdot \boldsymbol{v}_{\mathrm{I}}(t+t_0)}{q} \mathrm{e}^{-\mathrm{i}\boldsymbol{q}\cdot\boldsymbol{R}_{\mathrm{I}}(t+t_0)} \right) \left(\sum_{I=1}^{N} \frac{\boldsymbol{q} \cdot \boldsymbol{v}_{\mathrm{I}}(t_0)}{q} \mathrm{e}^{\mathrm{i}\boldsymbol{q}\cdot\boldsymbol{R}_{\mathrm{I}}(t_0)} \right) \right\rangle \tag{3.2}$$

and

$$C^{\mathrm{t}}(q,t) = \left\langle \left[\sum_{I=1}^{N} \left(\boldsymbol{v}_{\mathrm{I}}(t+t_0) - \frac{\boldsymbol{q} \cdot \boldsymbol{v}_{\mathrm{I}}(t+t_0)}{\boldsymbol{q} \cdot \boldsymbol{q}} \boldsymbol{q} \right) \mathrm{e}^{-\mathrm{i}\boldsymbol{q}\cdot\boldsymbol{R}_{\mathrm{I}}(t+t_0)} \right] \times \left[\sum_{I=1}^{N} \left(\boldsymbol{v}_{\mathrm{I}}(t_0) - \frac{\boldsymbol{q} \cdot \boldsymbol{v}_{\mathrm{I}}(t_0)}{\boldsymbol{q} \cdot \boldsymbol{q}} \boldsymbol{q} \right) \mathrm{e}^{\mathrm{i}\boldsymbol{q}\cdot\boldsymbol{R}_{\mathrm{I}}(t_0)} \right] \right\rangle \tag{3.3}$$

where the angled brackets denote the average over time origins t_0. Current correlation functions were obtained for the [1,0,0], [1,1,0] and [1,1,1] directions, with averaging over equivalent k vectors performed to improve accuracy (e.g. [1,0,0], [0,1,0] and [0,0,1] are equivalent).

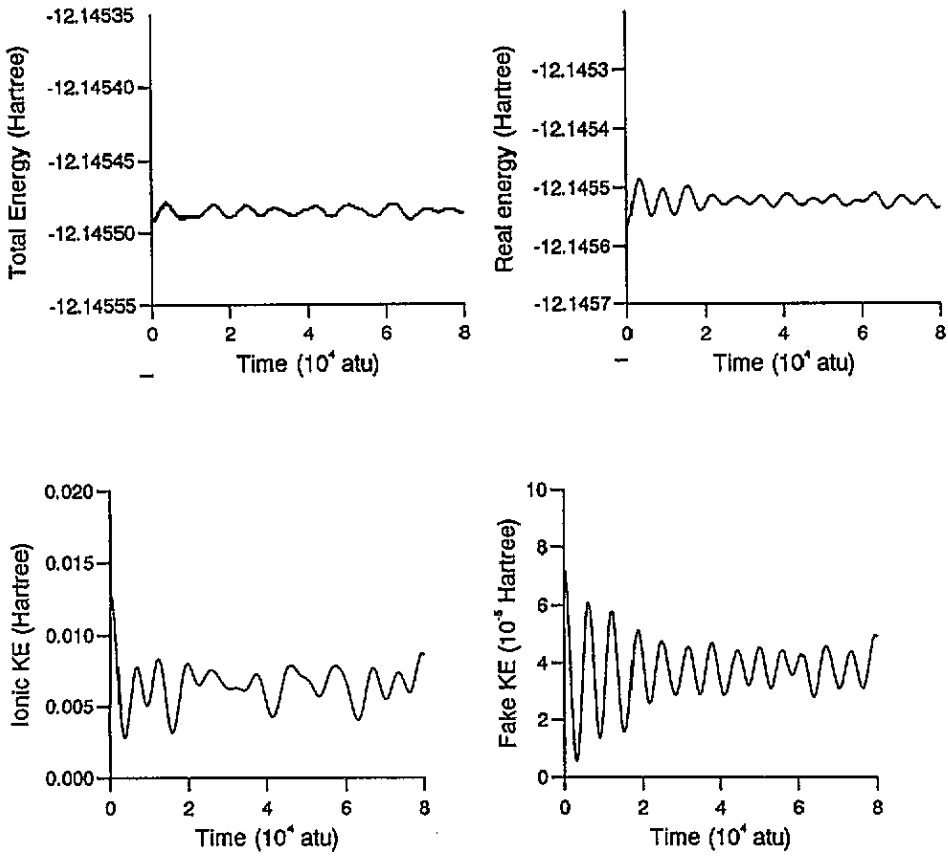

Figure 3. Various energies against time in the course of an MD simulation on a 54-atom system of sodium: the total energy, the total energy of the ionic system (the sum of the potential and ionic kinetic energies), the ionic kinetic energy and the 'fake kinetic energy' are shown. Note the differences in energy scales.

Due to the periodic boundary conditions, only phonons with certain wavelengths may be examined in these simulations. Specifically, if the simulation cell contains p unit cells in each direction then only phonons with polarization vectors of the form

$$k = \frac{2\pi}{L}[l, m, n] = \frac{2\pi}{a}\left[\frac{l}{p}, \frac{m}{p}, \frac{n}{p}\right] \qquad l, m, n \text{ integers} \tag{3.4}$$

may be observed, where a is the cell parameter and L the length of the simulation cell. We thus obtain a discrete set of points on the phonon dispersion curve; in order to sample the curves reasonably well, we did calculations on 54- ($p = 3$) and 128- ($p = 4$) atom systems.

Sample current correlation functions are shown in figure 4. The Fourier transforms have been obtained after windowing the correlation functions using the Blackman window [41]

$$W(t) = 0.42 + 0.5\cos\left(\frac{\pi t}{t_{\max}}\right) + 0.08\cos\left(\frac{2\pi t}{t_{\max}}\right). \tag{3.5}$$

The windowing function, while removing side lobes caused by the truncation of the correlation functions at $t = t_{\max}$, produces broadening of the peaks in the Fourier spectra. The phonon frequencies are thus taken as the frequencies at the peak maxima.

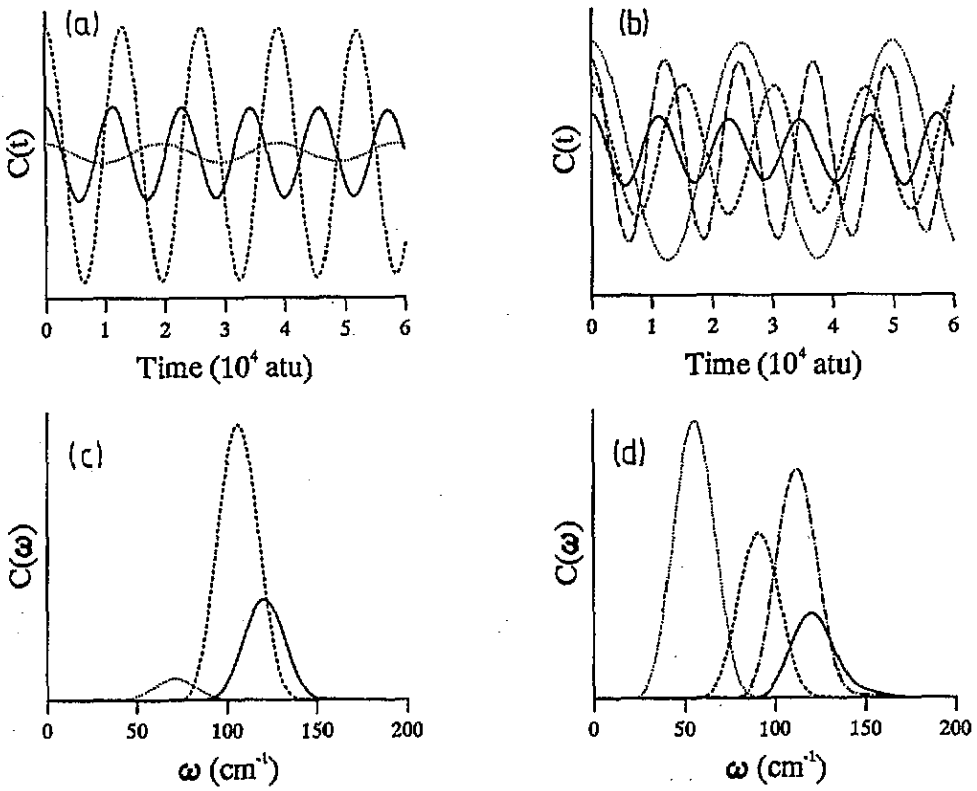

Figure 4. Time correlation functions and the associated spectra for full sodium. (*a*) and (*c*): the longitudinal $(k, 0, 0)$ $(k = 1, 2, 3)$ phonons in a 54-atom simulation; (*b*) and (*d*): the longitudinal $(k, 0, 0)$ $(k = 1\text{–}4)$ phonons in a 128-atom simulation.

The phonon dispersion curves from our simulations are compared with those obtained from neutron diffraction experiments [42, 43] in figure 5. The errors in the experimental data points range between $1\,\mathrm{cm}^{-1}$ and $3\,\mathrm{cm}^{-1}$ [42, 43]. The agreement between the simulation results and experiment is generally within this experimental error. The only large discrepancy is for the transverse $[q, q, 0]$ phonons (and then this is only for the points given by the 128-atom calculation). One would expect these phonons to be the most difficult to predict as (i) they are of low frequency—only about one and a half cycles are completed within the simulation time, and (ii) the transverse $[q, q, 0]$ modes are not degenerate and so there are two (partially overlapping) peaks in the associated current correlation function spectra. With a longer simulation these frequencies would probably be obtained to the same accuracy as those of the other phonons.

3.4. Timing and scaling properties

The 54-atom dynamics run was found to take 1.7 s per step on a Convex C2, allowing the whole 80 000 atu simulation to be performed in under one hour. The 128-atom calculation took 5.7 s per step. A CP step is seen to take 3.3 times as long for the 128-atom calculation as for the 54-atom calculation. If, as was hoped, the time scaled linearly with the system size then this figure would be 2.4; the scaling is therefore worse than linear. Looking at the timings for each routine in the program, one finds that everything scales linearly with

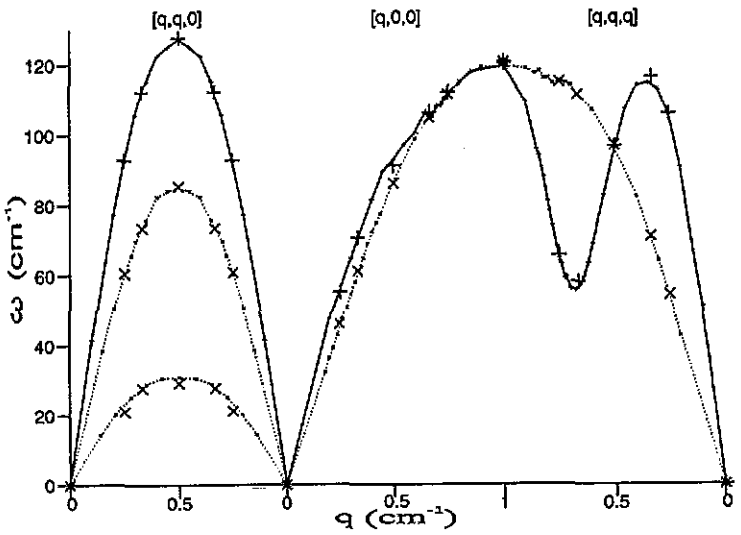

Figure 5. The phonon dispersion curve for sodium. The pluses (+) and crosses (x) show the phonon frequencies (longitudinal and transverse, respectively) calculated in this work from the 54- and 128-atom runs. The full and dotted curves are straight-line segments connecting the experimental data points [42, 43].

the system size, except for the calculation of the ionic structure factor (required for the electron–ion interaction and the forces on the ions). This scales as the number of ions times the number of basis functions, i.e. as the square of the system size. For 54-atoms, the calculation of the structure factor takes 0.6 s per step, whereas for 128 atoms it takes 2.8 s per step—it is beginning to dominate the entire calculation. It would seem, therefore, that for large systems we will get quadratic, as opposed to linear, scaling. This is, however, still an immense improvement on the scaling properties of the Kohn–Sham calculation. In electronic energy minimizations, or in calculations in which only a small number of ions are moved, the algorithm scales linearly.

3.5. Summary

This survey shows that the results obtained for solid sodium with the Perrot functional are excellent; in fact, they are better than those obtained from the Kohn–Sham calculation on the 54-atom system with only Γ point sampling (equivalent to sampling at three sets of k points on the primitive BCC cell [15]). The extraordinary aspect of the calculations is their low computational cost.

4. Stability analysis and conditioning the algorithm

The important property of the CP dynamics algorithm is that, under favourable circumstances, *the electronic state is automatically updated on the ground-state surface as the ions move.* The ion motion and the associated motion of the electronic state (the 'fake motion') are described by the coupled *classical* equations (1.7) and (1.8). The ions move with an average kinetic energy (temperature) determined by the thermodynamic state of the system being simulated, whereas under favourable circumstances, the temperature of the electronic degrees of freedom is much lower since the only motion is that required by adiabaticity. This implies,

therefore, that the *total classical* system (described by equations (1.7) and (1.8) remains in a non-equilibrium state for a long period. If the *total* system were ergodic, energy would be exchanged between the ionic and electronic degrees of freedom in such a way that the temperatures of the two subsytems would become equal (equipartition). The success of the CP method is due to the fact that the *total* system may remain in the two-temperature non-equilibrium 'adiabatic' state for long periods compared to the times required for the ions to explore appreciable regions of phase space.

4.1. Requirements for adiabaticity

The conditions for realizing the 'favourable circumstances' have been carefully discussed by Pastore and co-workers [44] in the context of normal (KS) CP dynamics. In this case the dynamics of the electronic system resembles that of a set of classical oscillators moving about a minimum position, which is the electronic ground state. In stable adiabatic runs the amplitude of these oscillations remains small. The oscillation frequencies are determined by the (real) electronic excitation energies ($\Delta\epsilon_{ij}$) and by the fake inertia (μ) as $(\Delta\epsilon_{ij}/\mu)^{1/2}$. The ion dynamics is also associated with a set of characteristic frequencies, whose density of states (as in normal MD) is approximately given by the Fourier transform of the velocity correlation function. Energy transfer between the ionic system and the fake dynamical system will be efficient if the range of ionic and fake system oscillation frequencies overlap, as this allows the necessary resonance condition. If this is the case adiabaticity will be poor. On the other hand, if a gap occurs in the electronic spectrum, the oscillation frequencies of the fake system can always be adjusted to be sufficiently high, so as to not overlap the ionic density of states by choosing the fake inertia to be small.

Since we have dispensed with orbitals (and hence any representation of the electronic excitations) in the present work it is clear that the stability of the dynamics we have found rests upon different principles. If the electronic coefficients ρ_g stray from their ground-state values ρ_g^{gs} by the amount $\Delta\rho_g$, then the character of (1.7) is to provide a restoring force on $\Delta\rho_g$, given by

$$\frac{\delta E}{\delta\rho}[\rho^{gs}+\Delta\rho]=\frac{\delta E}{\delta\rho}[\rho^{gs}+\Delta\rho]-\frac{\delta E}{\delta\rho}[\rho^{gs}]=\Delta\frac{\delta E}{\delta\rho}[\rho^{gs}] \tag{4.1}$$

(where we have used $\frac{\delta E}{\delta\rho}[\rho^{gs}]=0$: the equilibrium condition). If $\Delta\frac{\delta E}{\delta\rho}[\rho^{gs}]$ is linear in $\Delta\rho_g$ for small deviations from the ground state, then the coefficients perform harmonic motion about their ground-state values with characteristic frequencies

$$\omega_{\rho_g}=\left[\left(\Delta\frac{\delta E}{\delta\rho}[\rho^{gs}]\right)(\mu_g\Delta\rho_g)^{-1}\right]^{1/2}. \tag{4.2}$$

If $\Delta\frac{\delta E}{\delta\rho}[\rho^{gs}]$ is not linear in $\Delta\rho_g$ then the oscillations will not be harmonic and there will be a range of frequencies for each coefficient motion. This could be catastrophic for the CP algorithm.

Generally, the form of $\Delta\frac{\delta E}{\delta\rho}$ is very complicated, and we must make approximations in order to obtain an expression for it. If we assume that the perturbations from the ground-state density are very small, then we get

$$\Delta\frac{\delta E}{\delta\rho}=-\frac{\Delta\rho_g}{F(g)} \tag{4.3}$$

where $F(g)$ is the external susceptibility of the system of interest. The frequencies of the coefficient motions about the ground-state surface are therefore predicted to be

$$\omega_{\rho_g} = \sqrt{-1/F(g)\mu}. \tag{4.4}$$

Note that, because $F(g)$ is never infinite, the electronic frequencies can always be adjusted, by a suitable choice of μ, to avoid overlap between the electronic and ionic densities of states.

We will now show that the predictions of this simple model are in good accord with the behaviour observed for sodium.

4.2. Characteristic frequencies of the 'fake' motion

We examined the characteristic frequencies associated with the coefficient motion by calculating the correlation function of the coefficient velocities:

$$C_{vv}(g,t) = \frac{\langle \dot{\rho}_g(t+t_0)^* \dot{\rho}_g(t_0)\rangle}{\langle \dot{\rho}_g(t_0)^* \dot{\rho}_g(t_0)\rangle}. \tag{4.5}$$

Here the angled brackets denote an average over time origins t_0. As the theory in the last section suggests that coefficients with g vectors of the same magnitude will oscillate about their ground-state values with the same frequency, averaging was also performed over coefficients with such equivalent g vectors. In order to obtain the frequencies, the correlation functions were Fourier transformed to give their associated spectra $C_{vv}(g,\omega)$.

The correlation function spectra generally consist of one main peak with a frequency above $1000\,\mathrm{cm}^{-1}$. A typical example, for $g = (2\pi/L)\sqrt{5} = 0.587$, is shown in figure 6(*a*). No correlation function gives any structure above $5000\,\mathrm{cm}^{-1}$. Below $1000\,\mathrm{cm}^{-1}$ the peaks associated with the adiabatic motion of the coefficients at the characteristic frequencies of the ion motion occur; from the phonon dispersion curve of figure 5, we know that the ionic frequencies are in the range 0–$140\,\mathrm{cm}^{-1}$. The adiabatic peaks due to the ionic motion are much larger than those due to the non-adiabatic motion associated with departures from the ground state, since the ionic motion has a much larger amplitude (and the height of a peak is proportional to the *square* of the amplitude of the associated oscillation). The tails of these adiabatic peaks are seen in the spectrum shown in figure 6(*a*). As explained previously, the CP algorithm will break down if there is overlap in the frequencies of the ionic motion and the motion about the ground state. Thus the very region in which we are most interested in looking for non-adiabatic density oscillation frequencies ω_{ρ_g} is the region in which the associated peaks are swamped by the adiabatic spectrum.

The answer to this problem is to remove the adiabatic structure from the spectra by performing a CP run with fixed ions. This was done by starting a CP run using the ionic positions and coefficients from the end of a previous dynamics run. The ionic and coefficient velocities were both initially set to zero, and the ions were subsequently held fixed. As the coefficients at the end of a run will differ slightly from their ground-state values, when a CP run is started from this point the coefficients begin to oscillate about the ground state for the fixed nuclear configuration. The spectrum of the coefficient velocity correlation function for $g = (2\pi/L)\sqrt{5} = 0.587$ from a 20 000 atu fixed-ion CP run are shown in figure 6(*b*). The peak frequency associated with the non-adiabatic density oscillation occurs at the same frequency as in the moving-ion run; this was true for all ρ_g. There is no structure below $1000\,\mathrm{cm}^{-1}$ in any of the spectra from the fixed-ion run, as was expected, confirming that all the coefficient frequencies are higher than this value and well out of the range of the characteristic frequencies of the ionic motion.

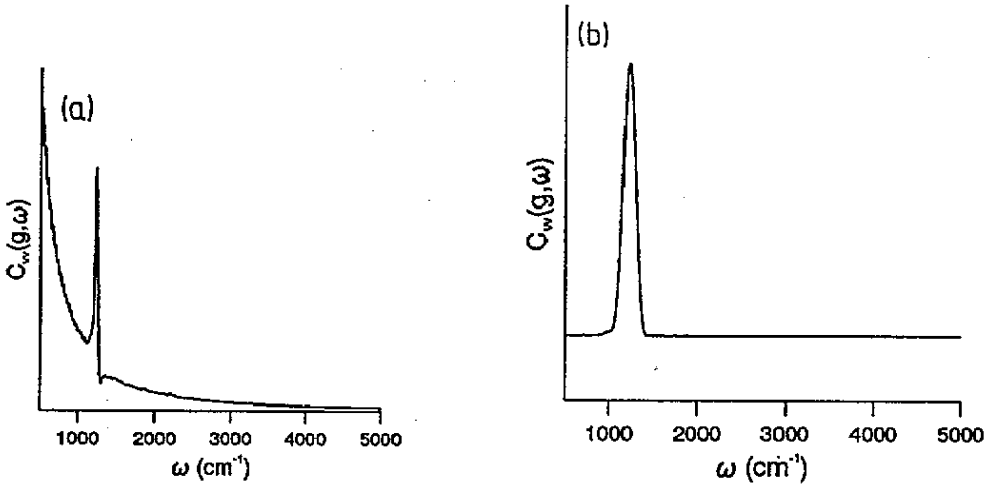

Figure 6. The spectra of the coefficient velocity correlation functions for the $g = 0.587\,\mathrm{au}^{-1}$ wavevector calculated (*a*) in moving-ion and (*b*) in static-ion simulations. The low-frequency part of the moving-ion spectrum is dominated by the adiabatic coefficient motion.

Coefficient oscillation frequencies identified in a fixed-ion run (on a small cell) are shown in figure 7. Also shown in the figure are the theoretical coefficient oscillation frequencies predicted from (4.4) using an approximation to the external susceptibility of the system of interest, namely the external susceptibility of a Hartree gas with the same electron density as sodium (i.e. the RPA curve of figure 1). We see that, even with this further simplification, the predicted frequencies agree remarkably well with those observed.

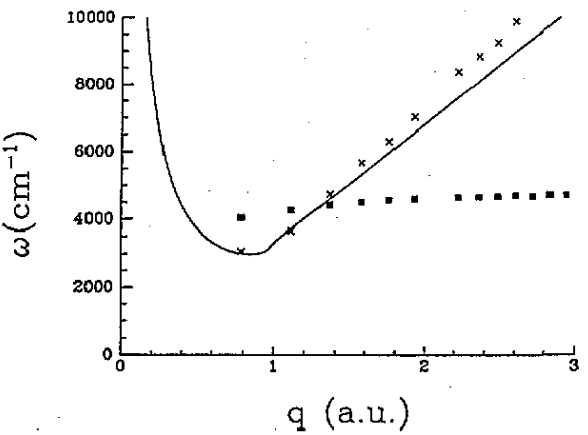

Figure 7. A comparison of the observed non-adiabatic coefficient oscillation frequencies (crosses, x) with the values predicted from equation (43) (full curve). The corresponding frequencies observed after conditioning are also shown (full squares). The data were obtained in calculations on a two-atom cell.

4.3. Conditioning

The finding that the oscillation frequencies are predictable, as outlined above, opens up the possibility of improving the efficiencies of the dynamics algorithm and the procedure used to minimize the electronic energy with respect to the electronic variables. The upper limit on the timestep δt in any dynamics algorithm is set by the requirement that the integration procedure be able to follow the fastest oscillations in the system. Usually, with a Verlet-type

algorithm, the period of the fastest oscillation should be at least ten times longer than δt. The period of the fastest coefficient oscillation in our system is about 1.3×10^{-14} s, so that our empirical finding of good energy conservation with $\delta t \simeq 10^{-15}$ s is consistent with this rule of thumb.

However, if we choose the 'fake masses', μ_g, such that

$$\mu_g = c/F(g) \tag{4.6}$$

all the coefficient frequencies become equal:

$$\omega_{\rho_g} = \sqrt{-1/c} \tag{4.7}$$

and by choosing c so as to minimize the coefficient frequencies, subject to the requirement that they remain comfortably outside the range of characteristic ion frequencies, we can maximize the timestep to a value determined by the frequencies of ionic motion. Note that, since $F(g) \propto g^{-2}$, $g \to 0$, the benefits of 'conditioning' the algorithm in this way will increase with system size, since the minimum value of g is inversely proportional to the cell length.

The same idea can be used to improve the efficiency of the electronic optimization step, required to find the ground state at the start of a run. A simple steepest-descent algorithm for this process is:

$$\rho_g(t + \delta t) = \rho_g(t) - \frac{\delta E}{\delta \rho_g}(t)\,\frac{\delta t^2}{\mu_g} \tag{4.8}$$

when written in terms of a 'time' that measures progress along the minimizing path. It is well known that this algorithm becomes painfully inefficient whenever the energy as a function of the $\{\rho_g\}$ has the shape of a long and narrow valley [45]. In the present context, this is equivalent to saying that the electronic frequencies span a wide range. By choosing the $\{\mu_g\}$ as in (4.6) we can greatly accelerate the convergence of the steepest descent procedure.

In practice, we approximated $F(g)$ by the value appropriate to the Hartree gas. In the test calculations illustrated in figure 7, we chose c so that the electronic frequencies were in the vicinity of $4500\,\mathrm{cm}^{-1}$. The range of electronic frequencies was narrowed, in the way predicted, so that all electronic frequencies were within $400\,\mathrm{cm}^{-1}$ of the target value. With the electronic frequencies conditioned in this way we performed runs on a 54-atom system and obtained energy conservation better than 10^{-5} hartrees and no significant transfer of energy between the ionic and fake systems over a run of 2000 steps with a timestep of 100 atu (2.5×10^{-15}) s. This is only a factor of about four shorter than the timestep that would be required in a classical MD run on this system. Similarly, conditioning the steepest descent algorithm increased the rate of convergence to the electronic ground state by a factor of two.

5. Conclusion

The purpose of this paper was to demonstrate the possibilities for *ab initio* MD simulation with an orbital-free density functional. Firstly, we have shown that explicit and simple forms for E_{KE}, which depend only on the density and which are adequate for simple metals, can be found. We have demonstrated that excellent results are obtained for solid sodium and

preliminary results show that results of similar quality are obtained for other simple metals in both the solid and liquid state; these results will be discussed in a future publication. The scope of the orbital-free density functionals is not yet established. We have already found that reasonable results are obtained for a semiconductor (Ge) with the simple second-order functional, in the sense that the diamond structure is (at least) locally stable and that the electron density shows maxima along the bond directions, suggestive of covalent bonding. However, it is likely that, to represent such systems accurately, a better functional will be required; the third-order functional discussed by Wang and Teter [19] is one possibility. Secondly, the low cost of evaluating the functional and the good scaling properties of the algorithm suggest that a considerably more complex improved functional (perhaps along the lines indicated by Wang and Teter [19]) could be used and still be much more efficient than KS for large systems. Thirdly, we have shown that the CP algorithm is extremely well behaved when using a functional of this type. We have analysed this property in detail and shown that the algorithm can be optimized to greatly improve its performance in both energy minimization and dynamics. With this optimized algorithm, calculations on large systems, containing over a thousand atoms, become viable. More complex orbital-free functionals present no difficulty in principle for the *ab initio* MD algorithm and should share the advantages we have detailed for the simple second-order functional.

Clearly, abandoning the wavefunction will ultimately limit the applicability of the method. The most obvious limitation is that there is no way of including the 'non-locality' of the pseudopotential in these calculations. At present, most pseudopotentials used in accurate KS calculations are non-local. Non-locality is believed to be essential to represent the interactions between electrons in a valence subshell with a core that contains no electrons with the same azimuthal quantum number [8]. However, non-local potentials are also used in other cases because softer potentials (which require a smaller plane-wave cutoff for convergence) may be constructed in this way by using larger values for the core radii. We should still be able to make progress with these elements with local potentials, the large basis set required with a local function should not present a major problem, given the efficiency of the electronic algorithm. If very small core radii are needed, non-linear core corrections can be made within our framework [46].

Acknowledgments

PAM would like to acknowledge helpful conversations with J-P Hansen and A Meroni, which provided the early stimulus for this work. The authors are very grateful to J Clérouin, G Zerah and G Ciccotti for organizing a most helpful workshop at CECAM, at which many of the ideas discussed here crystallized. The work was supported by SERC and the MOD (UK) under grant GR/H38256. It has also benefitted from further support from SERC under grant no. GR/H10276 and a studentship to MNP.

References

[1] Car R and Parrinello M 1985 *Phys. Rev. Lett.* **55** 2471
[2] Payne M C, Teter M P, Allan D C, Arias T A and Joannopolous J D 1992 *Rev. Mod. Phys.* **64** 1045
[3] Hohenberg P and Kohn W 1964 *Phys. Rev.* **136** 864
[4] Parr R G and Yang W 1989 *Density Functional Theory of Atoms and Molecules* (Oxford: Oxford University Press)
[5] Lundqvist S and March N H (ed) 1983 *Theory of the Inhomogeneous Electron Gas* (New York: Plenum)

[6] Dreizler R M and Gross E K U 1990 *Density Functional Theory* (Berlin: Springer)
[7] Kohn W and Sham L J 1965 *Phys. Rev.* **140** A1133
[8] Cohen M L and Chelikowsky J R 1988 *Electronic Structure and Optical Properties of Semiconductors* (Berlin: Springer)
[9] Pickett W E 1989 *Comput. Phys. Rep.* **9** 115
[10] Labanowski J K and Andzelm J W (ed) 1991 *Density Functional Methods in Chemistry* (Berlin: Springer)
[11] Perdew J P 1990 *Advances in Quantum Chemistry* **21** ed S B Trickey (New York: Academic)
[12] Rappe A, Rabe K, Kaxiras E and Joannopoulos J D 1990 *Phys. Rev.* B **41** 1227
[13] Troullier N and Martins J L 1991 *Phys. Rev.* B **43** 1993
[14] Car R and Parrinello M 1989 *Simple Molecular Systems at Very High Densities* ed. A Polian (New York: Plenum) p 451
[15] Remler D K and Madden P A 1990 *Mol. Phys.* **70** 921
[16] Galli G and Parrinello M 1992 *Phys. Rev. Lett.* **69** 3547
[17] Baroni S and Giannozzi P 1992 *Europhys. Lett.* **17** 547
[18] Perrot F 1992 Private communication
[19] Wang L-W and Teter M P 1992 *Phys. Rev.* B **45** 13197
[20] Blöchl P E and Parrinello M 1992 *Phys. Rev.* B **45** 9413
[21] Fois E S, Penman J N and Madden P A 1993 *J. Chem. Phys.* to be published
[22] Zerah G, Clérouin J and Pollock E L 1992 *Phys. Rev. Lett.* **69** 446
[23] Meroni A, Hansen J-P and Madden P A 1993 *J. non-Crystalline Solids* to be published
[24] Ashcroft N W 1982 *The Liquid State of Matter: Fluids, Simple and Complex* ed. E W Montroll and J L Lebowitz (Amsterdam: North-Holland)
[25] Harrison W A 1970 *Solid-State Theory* (New York: McGraw-Hill)
[26] Ashcroft N W and Mermin N D 1976 *Solid State Physics* (New York: Holt-Saunders)
[27] Pines D and Nozières P 1989 *The Theory of Quantum Liquids* vol 1 (New York: Addison-Wesley)
[28] Hafner J 1987 *From Hamiltonians to Phase Diagrams* (Berlin: Springer)
[29] Jones R O and Gunarsson O 1989 *Rev. Mod. Phys.* **61** 689
[30] Ceperley D M and Alder B J 1980 *Phys. Rev. Lett.* **45** 566
[31] Perdew J P and Zunger A 1981 *Phys. Rev.* B **23** 5048
[32] Vashista P and Singwi K S 1972 *Phys. Rev.* B **6** 875
[33] Topp W C and Hopfield J J 1973 *Phys. Rev.* B **7** 1295
[34] Rebonato R unpublished
[35] von Weizsäcker C F 1935 *Z. Phys.* **96** 431
[36] Jones W and Young W H 1971 *J. Phys. C: Solid State Phys.* **4** 1322
[37] Feder R and Charbneau H P 1966 *Phys. Rev.* **149** 464
[38] Aldhart W 1974 *Phys. Lett.* **47A** 91
[39] Nachtrieb N H, Cataland E and Weil J A 1952 *J. Chem. Phys.* **20** 1185
[40] Mundy J N 1971 *Phys. Rev.* B **3** 2431
[41] Allen M P and Tildesley D J 1987 *Computer Simulation of Liquids* (Oxford: Oxford University Press)
[42] Brockhouse B N, Arase T, Caglioti G, Rao K R and Woods A D B 1962 *Phys. Rev.* **128** 1099
[43] Woods A D B, Brockhouse B N, March R H, Stewart A T and Bowers R 1962 *Phys. Rev.* **128** 1112
[44] Pastore G, Smargiassi E and Buda F 1991 *Phys. Rev.* A **44** 6334
[45] Press W H, Flannery B P, Teukolsky S A and Vetterling W T 1986 *Numerical Recipes: The Art of Scientific Computing* (Cambridge: Cambridge University Press)
[46] Louie S G, Froyen S and Cohen M L 1982 *Phys. Rev.* B **26** 1738